Journal of Applied Fluid Mechanics, Vol. 17, No. 7, pp. 1430-1443, 2024.
Available online at www.jafmonline.net, ISSN 1735-3572, EISSN 1735-3645.
https://doi.org/10.47176/jafm.17.7.2442

Enhancing Axial Fan Noise Reduction through Innovative Wavy Blade Configurations

W. C. Qi, K. Cheng, P. C. Li and J. Y. Li†

School of Energy and Power Engineering, Xi'an Jiaotong University, Shaanxi, 710049, China

†Corresponding Author Email: Jyli@mail.xjtu.edu.cn

ABSTRACT

Noise is one of the key indicators to evaluate axial flow fans, and in many cases, it is also the only indicator for determining their suitability for use. In this study, a new method to reduce axial fan's noise was proposed for changing the section chord length to transform the blades of two axial fans with the same design parameters but distinct chord lengths to wavy blades. The aerodynamic calculations and noise reduction mechanism of the wavy configuration of the two fans were studied by combining CFD of large eddy simulation with the Lighthill acoustic analogy method. The results showed that the main mechanism contributing to noise reduction through wavy configuration was the promotion of transformation of the blade surface's layered vortex structure into an uncorrelated comb vortex structure. For fan blades with smaller chord lengths, the comb structure with low spanwise correlation was still maintained after the trailing edge, while for fan blades with larger chord lengths, the comb structure of the shedding vortex rapidly dissipated downstream of the trailing edge. Under the rated design conditions, the implementation of wavy leading edge blades resulted in noise reductions of 1.9 dB and 1.5 dB for the two fans, respectively, while wavy trailing edge blades yielded reductions of 2.6 dB and 2.1 dB, respectively. Furthermore, the adoption of wavy configuration induced a phenomenon of pressure increase and efficiency decrease in both axial fans at medium and low flow rates, with minimal impact at high flow rates. These outcomes underscored the superior noise reduction efficacy of the wavy trailing edge blades, offering a promising way for the noise reduction design of axial flow fans.

Article History

Received November 15, 2023
Revised January 23, 2024
Accepted February 7, 2024
Available online April 30, 2024

Keywords:

Wavy blades
Lighthill's acoustic analogy
Noise reduction
Flow field analysis
Large eddy simulation
Axial fans

1. INTRODUCTION

Axial flow fans have found extensive applications across various industries, including transportation, electric power, mining, and animal husbandry (Castegnaro, 2018). Noise plays a pivotal role in the performance of axial flow fans and, in many instances, serves as the determining factor for their usability. Currently, noise reduction strategies for axial flow fans primarily encompass the incorporation of silencers, utilization of sound-absorbing materials, and the implementation of sound aerodynamic design principles (Zhou et al., 2014; Zhai et al., 2016; Zhang et al., 2020; Lin et al., 2022). With the development of bionics, researchers have explored the low-noise mechanisms exhibited by certain bird wings, leading to the proposal of blade designs with a serrated leading edge (Hansen et al., 2010) and a serrated trailing edge (Cao et al., 2020) for the aerodynamic design of axial flow fans with low noise.

Research on noise reduction using serrated leading edges has a lengthy history spanning several decades. For instance, Hersh et al. (1974) designed a serrated leading edge referencing owl wing structures and found that it could reduce wing noise by 4-5 dB. Haeri et al. (2013) conducted numerical simulations of wing noise and determined that sinusoidal serrations on the leading edge altered leading-edge vortex structures could reduce three-dimensional wing turbulent noise by up to 3.717 dB for the configuration with maximum serration amplitude. Rao et al. (2017) experimentally demonstrated that owl-shaped leading-edge serrations passively controlled the transition from laminar to turbulent flow on the airfoil suction surface, thereby suppressing high-frequency vortex generation and reducing noise. Regarding the aerodynamic noise reduction for axial flow fan blades, Krömer et al. (2018) observed that the sinusoidal leading

NOMENCLATURE

BPF	blade passing frequency, fundamental frequency	LES	Large Eddy Simulation
CAA	Computational Aeroacoustics	MRF	Multiple Reference Frame
D	Diameter of the fan	N	number of time steps
f_{max}	the highest calculated noise frequency	rpm	revolutions per minute
Δf	frequency resolution of noise calculation	Δt	time step size
FFT	Fast Fourier Transform	x	blade section heights
h	blade height		

edge exhibited a further noise reduction effect as the volumetric flow rate increased, achieving a maximum reduction of 1.8 dB in free-inlet axial flow fans. Krömer et al. (2019) also investigated the aerodynamic noise reduction in skewed fans by modifying the leading edge serrations and reported that even for forward-leaning fans with low noise levels, serrated leading edges could further reduce aerodynamic noise. Tan et al. (2023) investigated the noise reduction effects of axial flow fan blades with a wavy leading edge coupled with a seagull-shaped airfoil and found that the biomimetic blade design effectively suppressed turbulent vortex generation and backflow, resulting in a 3.59 dB reduction in broadband noise. However, despite numerous studies addressing the noise reduction effects of leading edge serrations on blades, previous investigations involved directly cutting into the blade's leading edge, resulting in a deteriorated leading edge and altered blade section angle of attack, which adversely affected fan performance.

In addition to serrated leading edge blades, extensive research has been conducted on serrated trailing edge blades for noise reduction. Howe (1991, 1998) provided an early explanation of the noise reduction mechanism associated with serrated trailing edges and put forth formulas for predicting their noise reduction effectiveness. Zuo et al. (2019) discovered that a serrated profile could enhance the flow field near the trailing edge of the three-dimensional flow structure of the NACA-0018 airfoil, resulting in a reduction of aerodynamic noise and that the noise reduction effect became more pronounced as the amplitude of the serrated profile increased. Furthermore, Li et al. (2021) demonstrated that a slanting serrated trailing edge could effectively reduce noise in the high-frequency band and mitigate the peak noise levels in the low-frequency band. However, it is worth noting that previous research on serrated trailing edges often involved directly cutting the trailing edge of the blades, leading to disruptions in the airfoil's shape at the cutting section and having a detrimental impact on aerodynamic performance.

A wavy configuration blade was presented in this paper, which could improve the drawbacks of both the serrated leading and trailing edges by not cutting the streamlined airfoil shape and changing the stagger angle of the section. The wavy leading edge or trailing edge blades were generated by modifying the chord length of each section in a serrated way, which also brought about a ridged blade surface. A comprehensive numerical investigation was conducted into the noise reduction mechanisms of these newly proposed wavy leading and trailing edge blades for axial flow fans and the mechanism via which the wavy configuration affects the reduction of aerodynamic noise and fan's performance was analyzed.

2. NUMERICAL CALCULATION

2.1 Computational Domain

Two fans were designed to operate with the same designed pressure rise of 230 Pa at a flow rate of 13500 m³/h but at two different rotational speeds: 1100 rpm and 960 rpm. The chord of the two fans are quite different. This was done to study the noise reduction effect of the wavy configuration from a more general point, covering the typical blade shapes. The fan designed for 1100 RPM operation, known as Model 1100R (Fig. 1(a)), has a shorter chord length, while the fan designed for 960 RPM operation, referred to as Model 960R (Fig. 1(b)), has a longer chord length. The main geometric parameters of the

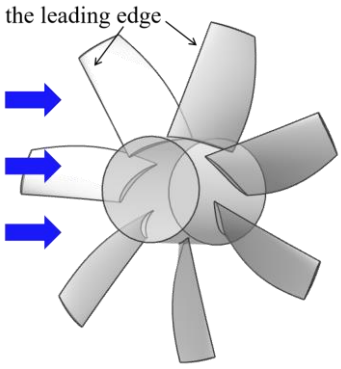

(a)

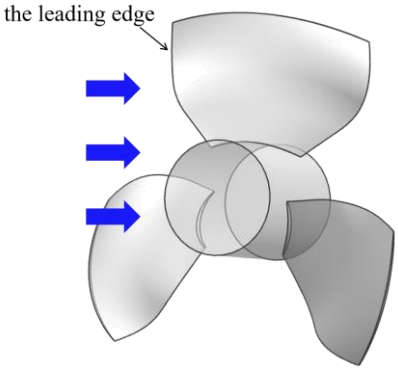

(b)

Fig. 1 Geometric models of the fans: (a) the 1100R model and (b) the 960R model

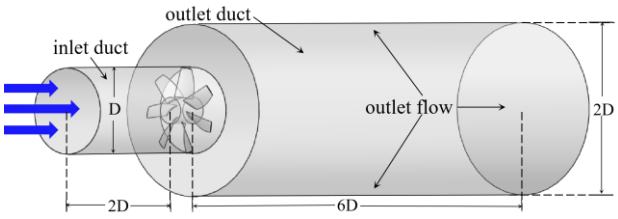

Fig. 2 Computational Fluid Domain of the fans

two fans are listed in Table 1. To ensure the full development of flow at the inlet and outlet of the fan while preventing the influence of boundary conditions and fluid backflow on computational accuracy, it is necessary to extend the numerical calculation domain of the fan. For numerical simulations, the computational domain extends upstream from the inlet and downstream from the fan's outlet (Fig. 2), as conducted by other researchers (Valencia et al., 2017). The inlet is positioned two times the fan diameter upstream, and the domain's outlet is located at a distance six times the fan diameter's length. To replicate the experimental outlet conditions, where air is discharged directly into the atmosphere, a duct with a diameter twice that of the rotor was attached to the fan's outlet.

The acoustic computational domain comprises several components, including the surface sound source, volume sound source, finite element acoustic propagation domain, and infinite element acoustic propagation surface (Fig. 3). Specifically, the interface between the exit of the fan and the inlet of the enlarged duct is considered the surface sound source, while the downstream region is designated as the volume sound source area. The acoustic computation domain can be chosen to be either equal to, or smaller than the size of the flow field computation domain. In this study, the acoustic computation domain was chosen to be smaller than the domain for flow field, as adopted by Zhang, et al. (2014). The volume sound source is chosen within 1.2D downstream from the fan outlet. To monitor acoustic properties, an acoustic monitoring point was placed 1 meter downstream from the hub center.

2.2 Computational Models

The flow field simulations were conducted using the Ansys CFX software. Initially, a steady flow simulation was performed on the computational domain using the *k-ω* SST turbulence model. The simulation comprised one blade passage for the rotor and the entire flow field within the upstream and downstream ducts, with the casings specified as solid walls. The rotor domain was treated using the Multiple Reference Frame (MRF) method. Wall boundaries were subjected to no-slip conditions, and the Mixing-Plane stage condition was applied to the interfaces between the rotor and ducts. Inlet velocity and outlet pressure boundary conditions were assigned to the domain's inlet and outlet, respectively. Convergence was deemed achieved either when the residuals dropped below 10^{-6} or when their monitoring values stopped to decrease.

The steady flow field results obtained from the simulation were used as initial values for the subsequent transient simulation. Many studies (Lele et al., 2010; Cavalieri et al., 2011; Shur et al., 2011; Liu et al., 2013) have shown that the identification and capture of turbulent vortices in the flow field by Large Eddy Simulation (LES) is more accurate, and it is feasible to be used in the study of flow-field noise. Therefore, LES was conducted to

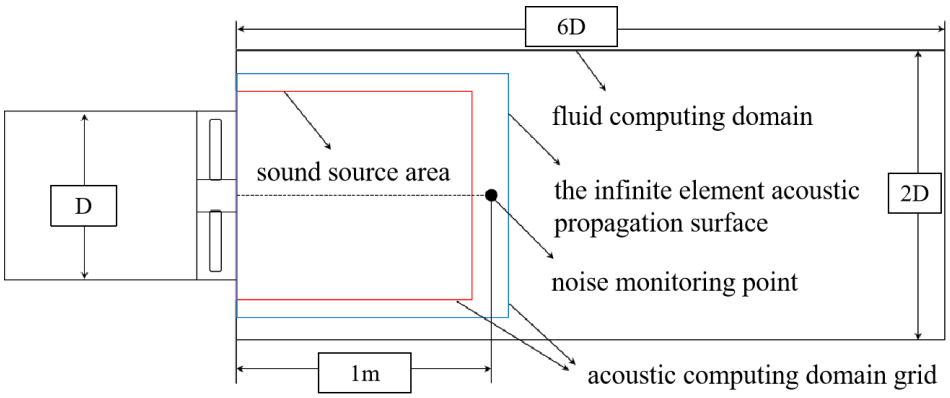

Fig. 3 Acoustic calculation domain of the fans

Table 1 Geometric parameters of two fans

	1100R			960R		
Relative blade height: *x*/h	0	0.5	1	0	0.5	1
Stagger angle (°)	59.03	37.49	14.55	45.3	39.15	29.5
Chord length (mm)	162.73	136.53	95.47	153.41	343.29	372.22
Maximum thickness (mm)	12.37	9.43	6.48	11.24	7.85	6.4
Number of blades	7			3		
Axial length (mm)	115.6			232.3		
Tip clearance (mm)	5			5		
Diameter of the fan (mm)	710			710		

model the unsteady flow fields, utilizing the Smagorinsky subgrid-scale model. The transient rotor-stator method was applied at the interface between the moving and stationary components. To achieve a maximum noise calculation frequency of 3500 Hz, a time step of 1.43×10^{-4} s was chosen for both fans, as per Eq. (1) (Nyquist 1928). For each time step, a maximum of 30 iterations were performed proceeded to the next step either when the residuals dropped below 10^{-4} or when the maximum iteration count was reached. Data recording started once the calculations reached a state of periodic solutions. Given the selected noise resolution of 5 Hz, as per Eq. (2) (Nyquist 1928), the number of steps for the unsteady simulation results amounted to 1400 for both fans.

$$f_{\max} = \frac{1}{2\Delta t} \tag{1}$$

$$\Delta f = \frac{1}{N\Delta t} \tag{2}$$

where, $f_{\max}$ represents the highest calculated noise frequency, Hz; Δf is the frequency resolution of noise calculated, Hz; and N indicates the number of CFD calculation steps.

When the unsteady simulation was completed, the acoustic calculation was performed. A hybrid Computational Aeroacoustics (CAA) approach was employed for the computation of noise and the prediction of far-field sound propagation, which is mainly based on the Lighthill acoustic analogy method to convert the flow field information into sound source information. Finally, the acoustic finite element and infinite element methods were used to calculate the sound propagation and predict the far-field radiation sound field (Sandboge et al., 2006). The steps are as follows:

(1) The flow field data obtained at each time step was output in the "ensightgold" format.

(2) Utilizing the ICFD analysis module, the acoustic analogy method was used to extract time-domain acoustic source data from the internal flow field and subsequently mapped onto the acoustic grid. Fast Fourier transform (FFT) was applied to convert the time-domain acoustic information into acoustic data in the frequency domain. Surface sources representing the acoustic emissions from the fan were incorporated using data from the interface, while the outlet flow region in the enlarged duct was treated as volume sources.

(3) Lastly, far-field noise calculations were conducted using frequency response analysis to obtain far-field noise data. The flow chart for noise calculation is shown in Fig. 4.

2.3 Computational Grid Design

Grid independence validation of the simulations was conducted by incrementally increasing the number of grids (Table 2). Comparative analysis with the highest grid count revealed that when the total grid count reached 3.13 million (comprising 2.16 million nodes in the rotor domain and 0.97 million nodes in the inlet and outlet extensions), further increments in grid numbers only

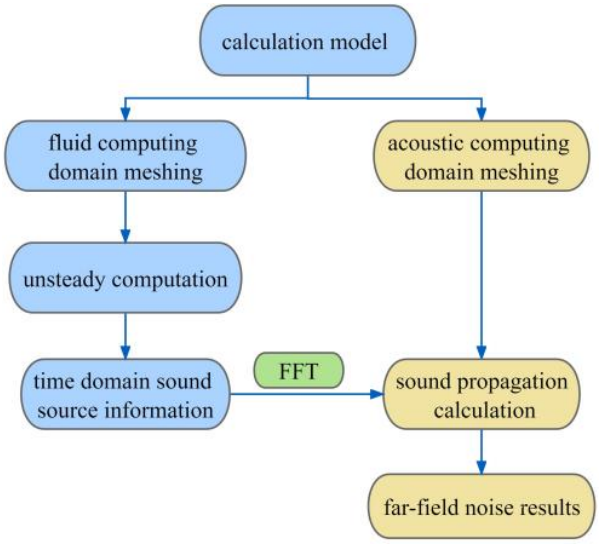

Fig. 4 Acoustical calculation flow chart

Table 2 Grid independence test

	Number of grids	Changes of total pressure	Changes of total pressure efficiency
1	950,000	2.317%	0.680%
2	1,660,000	0.980%	0.479%
3	2,300,000	0.369%	0.101%
4	3,130,000	0.006%	0.020%
5	3,960,000	0.001%	0.013%
6	4,860,000	0	0

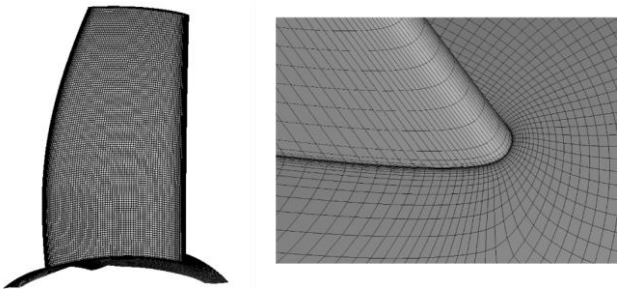

Fig. 5 Grid distribution of the blade

resulted in slight changes to the fan's total pressure and total pressure efficiency. As a result, the grid containing 3.13 million nodes was selected for the steady simulations. For unsteady simulations using LES, a significantly denser grid was employed, totaling 9.37 million nodes. To ensure a y+ value of less than 1 for the near-wall mesh, the first-layer mesh height for the 1100R fan was set to 0.0085 mm, while for the 960R fan, it was 0.01 mm. A total of 15 layers were distributed adjacent to the wall boundary to ensure accurate capture of wall pressure fluctuations, which are critical for acoustic calculations. The grid distribution used in the LES around the blade and the zoomed-in leading edge is shown in Fig. 5.

At the design flow rate of 13500 m³/h, the pass frequencies (BPFs) at the noise monitoring point were calculated and compared between the 1100R fan and the 960R fan with theoretical data determined by their respective

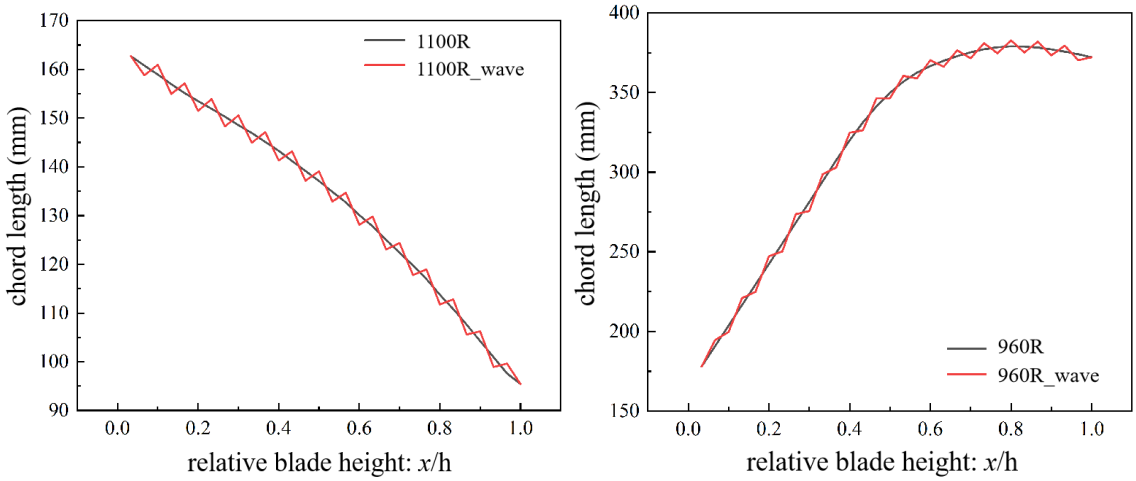

(a) (b)

Fig. 6 Chord length distribution of two fans along blade height: (a) 1100R, (b) 960R

Table 3 Calculation results of the fan noise

Fans	Simulated BPF(Hz)	Theoretical BPF(Hz)	Relative errors
1100R	129.8	128.3	1.2%
960R	46.8	48.0	2.5%

rotational speeds (Table 3). The simulated noise levels at the monitoring point are also presented in Table 3. The computational results reveal that the pass frequency for the 1100R fan is 129.8 Hz, with a simulated noise level of 78.53 dB, while the pass frequency for the 960R fan is 46.8 Hz, with a noise level of 78.25 dB. These calculated BPFs closely align with the theoretical values, with relative errors in the BPFs for both fans being only 1.2% and 2.5%, respectively.

2.4 Wavy Configuration Modeling

Thirty cross-sections were strategically chosen along the blade height to create wavy leading and trailing edges by adjusting the chord length at different cross-sections, thus preserving the airfoil shape of each section. The amplitude of these wavy leading and trailing edges was set to 2% of the respective chord length. The chord distribution along the blade height for the 1100R fan and the chord distribution for the 960R fan is shown in Fig. 6(a) and Fig. 6(b), respectively.

3. NOISE REDUCTION MECHANISM OF THE WAVY LEADING EDGE

3.1 Models of Wavy Leading Edge Fans

The blades with wavy leading edges are shown in Fig. 7, indicating evident ridges on the blade surfaces near the leading edges, while the surfaces near the trailing edges of the blades remain comparatively smooth.

3.2 Influence of the Wavy Leading Edge on Fan Performances

Figures 8 and 9 illustrate the performance curves for the initial 1100R and 960R fans, as well as their counterparts

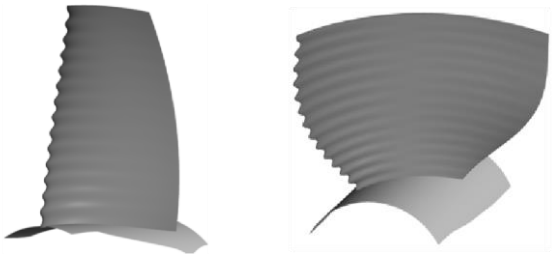

(a) (b)

Fig. 7 Geometric models of the wavy leading edge blades: (a) 1100R_wary leading edge and (b) 960_wavy leading edge

equipped with wavy leading edges. In general, the presence of wavy leading edges has a certain impact on the performance of both fans, particularly at lower flow rates, resulting in increased pressure and decreased efficiency. For the 1100R fan with wavy leading edges, the maximum reduction in efficiency occurs at low flow rate of 10500 m³/h, amounting to 1.66%, while there is a maximum pressure increase of 2.6 Pa. Similarly, the 960R fan equipped with wavy leading edges has a 1.52% reduction in efficiency and a 4.9 Pa pressure increase at low flow rate of 10500 m³/h. These findings indicate that the wavy leading edge design enhances pressure performance under low flow conditions. Conversely, for medium to high flow rate conditions, the 1100R fan with wavy leading edges exhibits only slight changes in efficiency, with pressure levels remaining similar to the model without the leading edge treatment. For the 960R fan with wavy leading edges, a minor pressure increase at high flow rates accompanied also by a reduced decline in efficiency is observed.

Figure 10 displays contour maps of the outlet pressure for the 1100R fan with wavy leading edge structures at both the rated flow rate (13500 m³/h) and a low flow rate (10500 m³/h) when the fan runs at the 1400 time step after the periodic operation and calculation have been reached. At the rated conditions (Fig. 10(a)), the regions with high

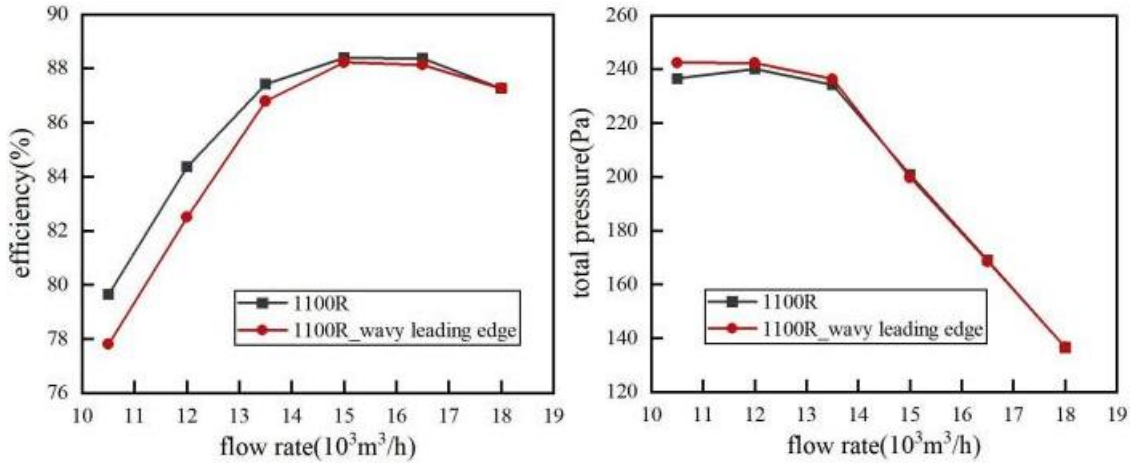

(a) (b)

Fig. 8 Performance comparison between 1100R_wavy leading edge and 1100R: (a) efficiency and (b) total pressure

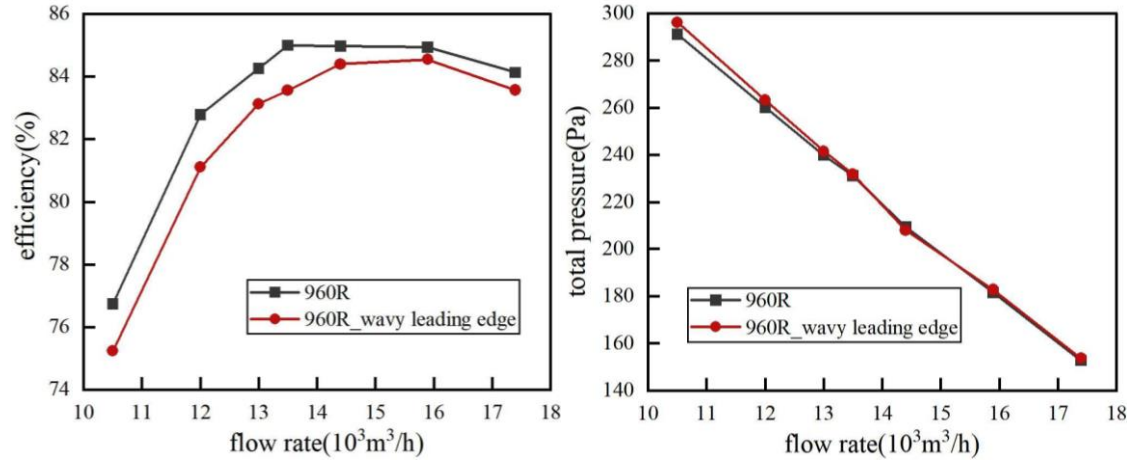

(a) (b)

Fig. 9 Performance comparison between 960R_wavy leading edge and 960R: (a) efficiency and (b) total pressure

pressure are comparable for both fans, but at the low flow conditions (Fig. 10(b)), a distinct high-pressure region emerges in the middle of the blade height for the modified 1100R fan. This suggests that the wavy leading edge blades enhance the blade's lifting force, resulting in increased outlet pressure, particularly at medium to low flow conditions. Figure 11 presents contour maps of the outlet pressure for the 960R fan, comparing configurations with and without wavy leading edge structures, at both the rated flow rate (13500 m³/h) and a low flow rate (10500 m³/h). The figures were also obtained at the 1400 time step after the periodic calculation being reached. With the inclusion of wavy leading edges, the modified 960R fan exhibits expanded areas with elevated outlet pressure. In contrast to the 1100R fans, the increase in outlet pressure with wavy leading edges in the 960R fan is concentrated mainly in the upper-middle section of the blade height, with this trend becoming more pronounced at lower flow conditions.

3.3 Influence of the Wavy Leading Edge on Noise

Under rated operating conditions, the calculated noise levels for all four fans at the monitoring point are summarized in Table 4. The results show that the overall noise level of the 1100R fan is reduced by nearly 1.9 dB

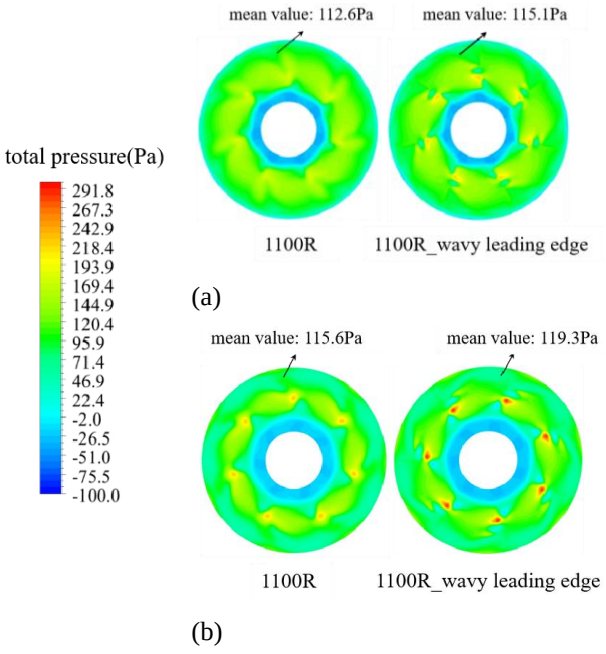

Fig. 10 Outlet pressure of 1100R and 1100R_wavy leading edge under different flow rates: (a) 13500 m³/h and (b) 10500 m³/h

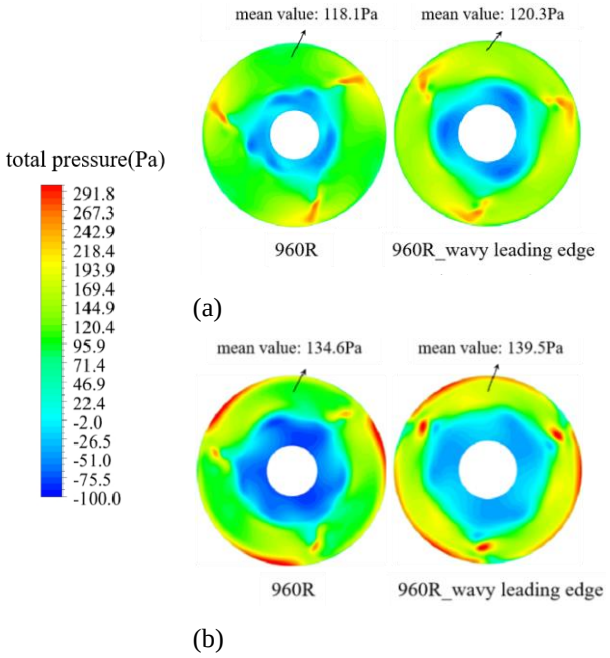

Fig. 11 Outlet pressure of 960R and 960R_wavy leading edge under different flow rates: (a) 13500 m³/h and (b) 10500 m³/h

Table 4 Noise reduction of the wave leading edge

Fans	Noise (dB)	Noise at 1BPF (dB)
1100R	78.5	60.9
1100R_wavy leading edge	76.6	58.7
960R	78.3	57.7
960R_wavy leading edge	76.8	56.4

after adding the wave leading edge, and the noise level at 1BPF is reduced by about 2.2 dB. Similarly, for the 960R fan, the addition of the wavy leading edge results in an overall noise reduction of approximately 1.5 dB, with a reduction of about 1.3 dB at 1BPF.

Figure 12 presents the sound pressure frequency spectra for both the 1100R and 960R fans, both with and without wavy leading edges. The inclusion of wavy leading edges results in an overall reduction in noise across the entire frequency range considered in the calculations. For the 1100R fan with wavy leading edges, there is a slight reduction in noise levels in the low-frequency band before 2BPF (254 Hz), followed by an

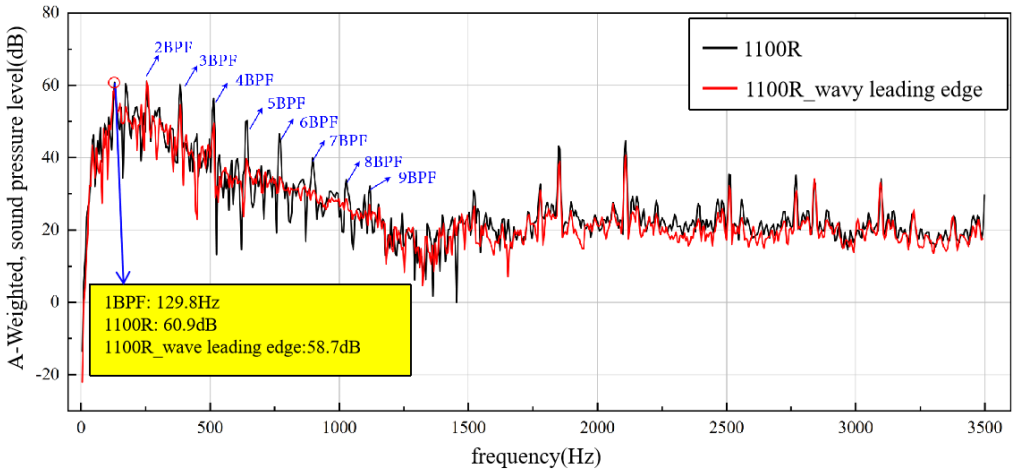

Fig. 12 A-Weighted, sound pressure level of fans: (a) 1100R and 1100R_wavy leading edge, and (b) 960R and 960R_wavy leading edge

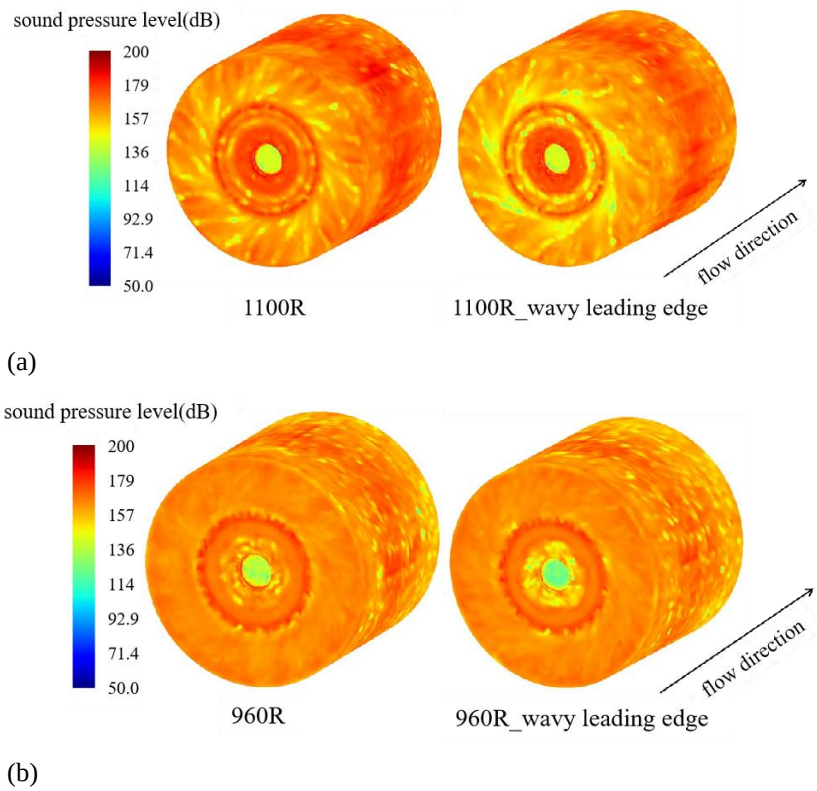

Fig. 13 Sound pressure level of fans at 1BPF: (a) 1100R and 1100R_wavy leading edge (129.8Hz), and (b) 960R and 960R_wavy leading edge (46.8Hz)

increase of approximately 3 dB at 2BPF. The most significant noise reduction occurs in the mid-frequency band, ranging from 2BPF to 1200 Hz, with this effect becoming more pronounced at higher BPFs. However, in the frequency range exceeding 1200 Hz, the reduction in noise becomes less evident. In contrast, for the 960R fan, the addition of wavy leading edges leads to noise reduction at BPFs in the mid-low frequency range from 1BPF (46.8 Hz) to 5BPF (327.6 Hz), with the maximum reduction of approximately 8 dB occurring at 2BPF (93.2 Hz). In the mid-high frequency range from 7BPF to 3500 Hz, noise reduction is significantly observed in the frequency range of 500-1000 Hz.

In summary, the wavy leading edge design demonstrates a notable noise reduction effect on both the 1100R and 960R fans, with a particularly pronounced reduction in the 500-1000 Hz frequency range, and can also attenuate tonal noise at specific harmonics.

Figure 13 displays sound pressure contour maps at the 1BPF for different fans, from the fan outlet to the far-field noise plane. Due to a sudden increase in through-flow area after the fan outlet, the sound pressure level initially rises and then decreases along the axial direction as the high-speed airflow requires time to fill the enlarged duct. On the fan's exit section, it is evident that the introduction of a wavy leading edge for the 1100R fan leads to a significant reduction in sound pressure levels in the upper portion of the blade, indicating that the noise reduction primarily affects the upper section of the blades. Conversely, for the 960R fan, the addition of the wavy leading edge results in a less substantial reduction in sound pressure levels in the upper portion of the blade compared to the 1100R model, but there is a significant reduction in sound pressure levels in the lower section of the blade.

The generation, development, and shedding of vortices on and from fan blades play a crucial role in influencing their noise characteristics (Koca et al., 2018). A mechanism accounting for the reduction in fan's noise involves diminishing the spreading correlation of shedding vortices, as demonstrated by the serrated structure (Zhou et al., 2022). Figure 14 provides insight into the vortex structures on the blade surfaces and within the wake of the 1100R and 960R fans, both with and without wavy blades, based on the Q criterion ($Q=4\times10^{-5}$). For the 1100R fan, layered vortices encompass the leading portion of the blade suction surface initially and then start to separate from the 1/2 chord position. The shedding vortices are poorly correlated with the blade trailing edge, and transform to comb vortex structures in the downstream of the blade. Upon adding the wavy leading edge, the layered vortices begin to transform into comb vortices at the 1/3 chord position, and the comb vortices are much sparser in the downstream than those of the initial blade. These sparsely distributed comb vortices indicate that implementing a wavy leading edge on the fan blade effectively weakens the intensity of the comb vortices in the wake of the wavy blades. The trend is particularly pronounced in the upper portion of the blade, possibly explaining the more significant reduction in sound pressure levels observed in the upper section of the blade for the 1100R fan with a wavy leading edge. In

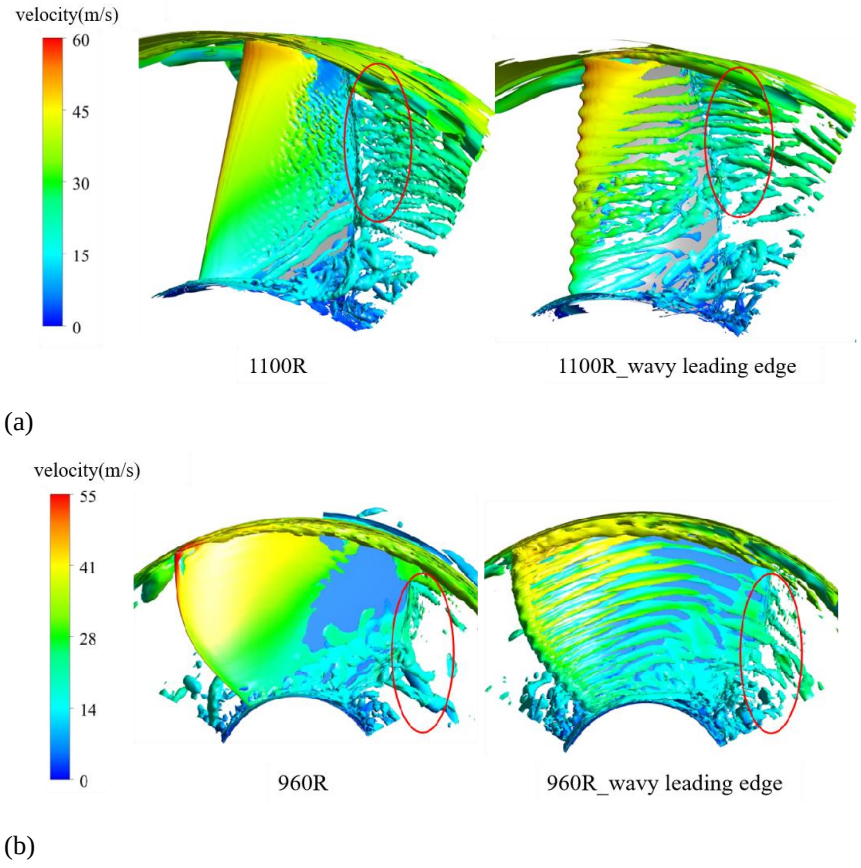

Fig. 14 Comparison of the surface vortex and wake vortex structures of fans: (a) 1100R and 1100R_wavy leading edge, and (b) 960R and 960R_wavy leading edge

contrast, the 960R fan possesses a distinct blade shape compared to the 1100R fan, resulting in different vortex structures within the duct. The addition of a wavy leading edge to the 960R fan leads to a less pronounced reduction in vortex strength and quantity of the comb vortices, compared to the 1100R fan. Although layered vortices on the blade surface of the 960R fan also transition into comb vortices, the reduction in shedding vortex scale is only noticeable in the region near the blade root where the chord length is smaller. In summary, the utilization of the wavy leading edge structure promotes the transformation of layered vortex structures on the blade surface into comb vortices and significantly diminishes the spanwise correlation and density of the shedding comb vortices, contributing to the reduction in fan noise.

4. NOISE REDUCTION MECHANISM OF THE WAVY TRAILING EDGE

4.1 Models of Wavy Trailing Edge Fans

Similar to how birds like owls employ serrated structures on their trailing edges for silent flight, the blades of both the 1100R and 960R fans were adapted at their trailing edges using the chord distribution shown in Fig. 6. In addition, similar to the wavy leading edges, these wavy trailing edge blades also incorporate surface ridged structures, as shown in Fig. 15.

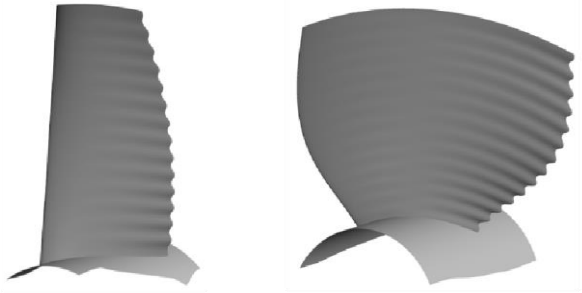

Fig. 15 Geometric models of the wavy trailing edge blades: (a) 1100R_wary trailing edge, and (b) 960_wavy trailing edge

4.2 Influence of the Wavy Trailing Edge on Fan Performances

Numerical simulations of the fans equipped with wavy trailing edges were performed to characterize the performance of both the 1100R and 960R fans (Fig. 16 and 17). The wavy trailing edges results in a certain reduction in both efficiency and pressure for both fans, particularly evident at medium to low flow rates. For the 1100R fan with wavy trailing edges, the maximum drop in efficiency is observed at an operating condition of 10500 m^3/h, with a reduction of 3.1%. Additionally, at a flow rate of 12000 m^3/h, the maximum pressure drop reaches 6.5 Pa. For the 960R fan equipped with wavy trailing edges, the

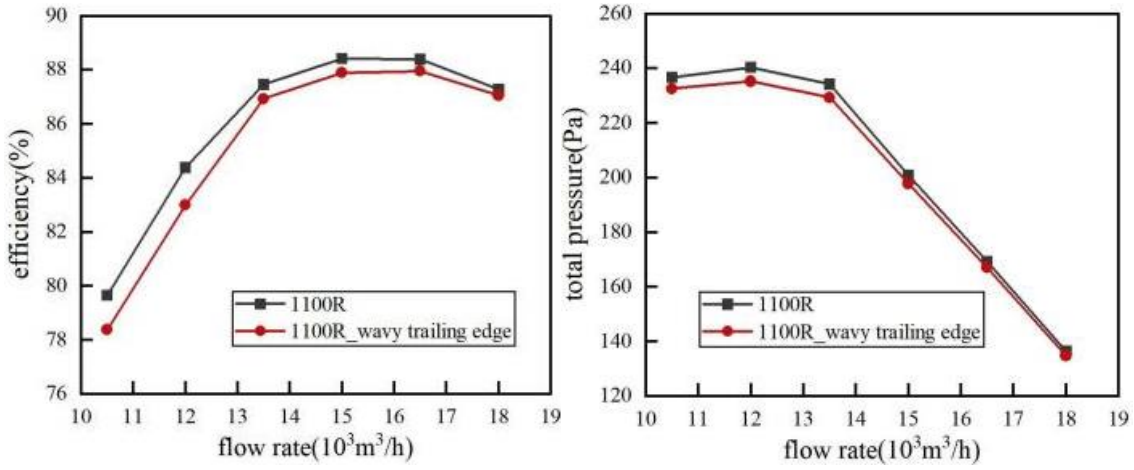

(a) (b)

Fig. 16 Performance comparison between 1100R_wavy trailing edge and 1100R: (a) efficiency, and (b) total pressure

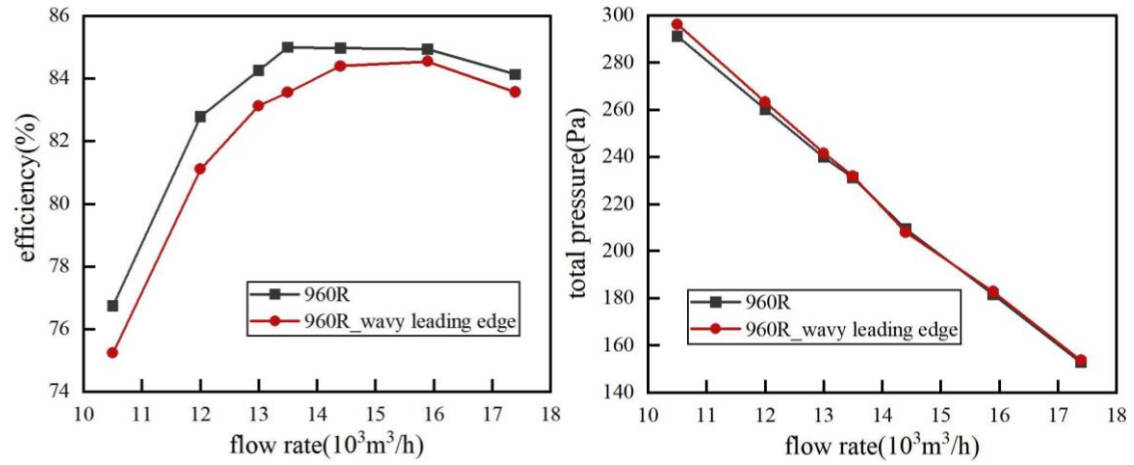

(a) (b)

Fig. 17 Performance comparison between 960R_wavy trailing edge and 960R: (a) efficiency, and (b) total pressure

Table 5 Noise reduction of the wave trailing edge

Fans	Noise (dB)	Noise at 1BPF (dB)
1100R	78.5	60.9
1100R_wavy leading edge	75.9	57.1
960R	78.3	57.7
960R_wavy leading edge	76.2	55.9

maximum efficiency decrease amounts to 1.7% at an operating condition of 10500 m³/h, with a maximum pressure drop of 4.9 Pa. Importantly, as the flow rate increases, the influence of the wavy trailing edges on the efficiency and pressure of both fans gradually diminishes.

4.3 Influence of the Wavy Trailing Edge on Noise

Numerical calculations of noise at rated conditions for both fans equipped with wavy trailing edges are summarized in Table 5. The inclusion of wavy trailing edges results in a significant reduction in overall noise levels for both the 1100R and 960R fans. Specifically, the 1100R fan shows an overall noise reduction of 2.6 dB, along with a 3.8 dB reduction in tonal noise at 1BPF. Meanwhile, the 960R fan achieves an overall noise reduction of 2.1 dB, coupled with a 1.9 dB reduction in tonal noise at 1BPF. In terms of noise reduction effectiveness, the wavy trailing edge appears to outperform the wavy leading edge, both in terms of overall noise reduction and tonal noise reduction at 1BPF.

Figure 18 shows the sound pressure spectra for fans with and without wavy trailing edges. For the 1100R fan, the wavy trailing edge leads to a general reduction in noise across the entire frequency spectrum, with the most significant effect observed in the 0 to 1000 Hz range, particularly within 500 - 1000 Hz, as compared to higher frequencies above 1000 Hz. Notably, the wavy trailing edge also effectively reduces tonal noise, with the most substantial reduction occurring at 2BPF, reaching 10.3 dB. For the 960R fan, the noise reduction impact of the wavy trailing edge primarily manifests in the frequency range below 2500 Hz, with the most significant reduction

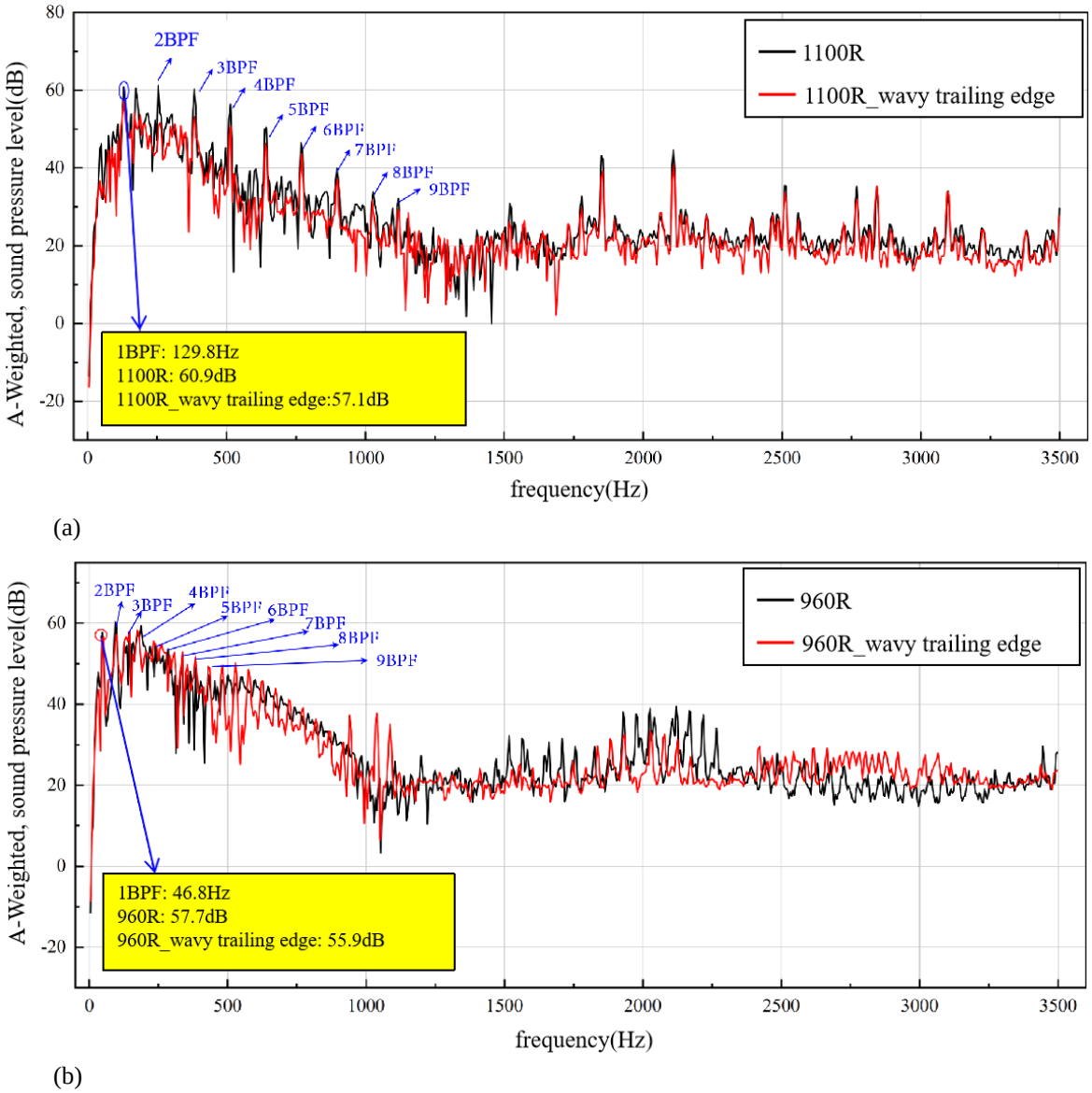

Fig. 18 A-Weighted, sound pressure level of fans: (a) 1100R and 1100R_wavy trailing edge, and (b) 960R and 960R_wavy trailing edge

observed in the 500-1000 Hz range. However, there is a slight increase in single-tone noise within this range, while noise levels are elevated in the range above 2500 Hz. Octave spectra can provide a clearer depiction of the broadband noise characteristics.

The effect of the wavy trailing edge on the sound pressure level in different frequency bands can be observed more clearly by the 1/3 octave spectra. Figure 19 shows the 1/3 octave spectra for the 1100R and 960R fans. For the 1100R fan, we observed a reduction in broadband noise across the entire frequency spectrum, with the most significant reduction occurring in the 0-800 Hz range, approximately 3.9 dB. Meanwhile, for the 960R fan with a wavy trailing edge, the reduction in broadband noise mainly occurs in the frequency bands of 400-800 Hz and 1400-2200 Hz, with the maximum reduction amounting to about 5.6 dB. However, in other frequency ranges, there is a slight increase in broadband noise for the 960R fan.

Figure 20 illustrates the variations in vortex structures induced by the wavy trailing edges, with the Q criterion set at 4×10^{-5}. When wavy trailing edges are added to the 1100R fan blades, the layered vortices on the blade's suction surface disappear shortly after the leading edge, and comb vortices are promoted by the ridge structure on the rear part of the blade surface. These shedding vortices flow into the wake of the blade, maintaining the comb structures downstream, indicating that the wavy trailing edge effectively reduces the correlation of shedding vortices, making it a primary contributor to noise reduction. In the case of the 960R fan with wavy trailing edges, the changes in vortex structures are similar to those observed in the 1100R fan blades after the addition of wavy trailing edges. The layered vortices near the leading edge vanish, and comb vortices are generated in the rear half of the blade. However, the vortex structure in the wake is different. The comb vortices dissipate or fragment rapidly into smaller ones downstream of the blade. This fragmentation of larger vortices near the blade root is more evident, which is the key factor contributing to noise reduction.

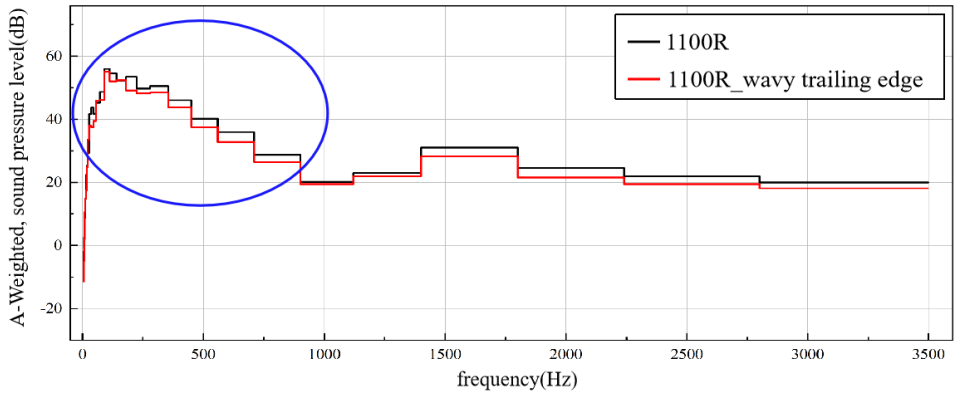

(a)

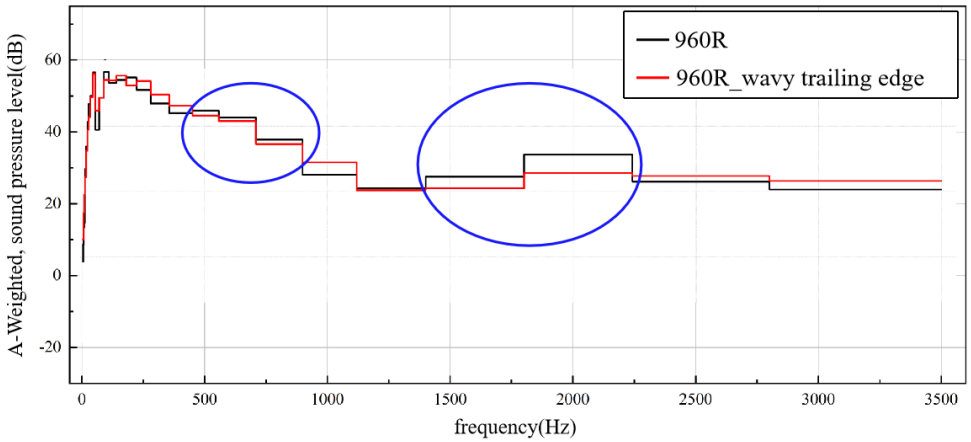

(b)

Fig. 19 A-Weighted, 1/3 octave spectra of fans: (a) 1100R and 1100R_wavy trailing edge, and (b) 960R and 960R_wavy trailing edge

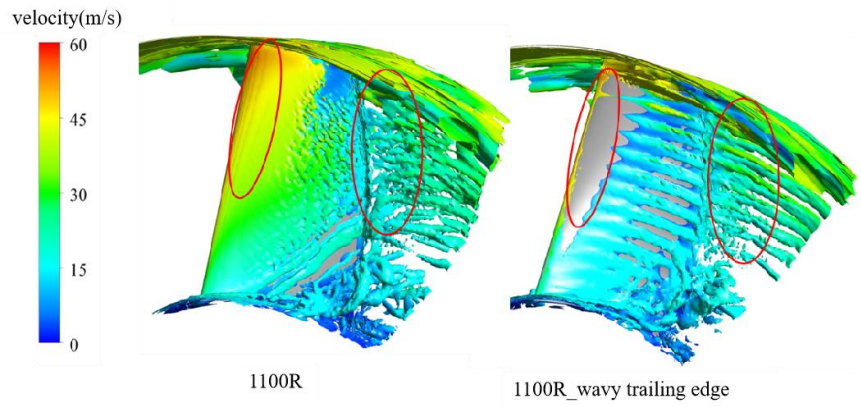

(a)

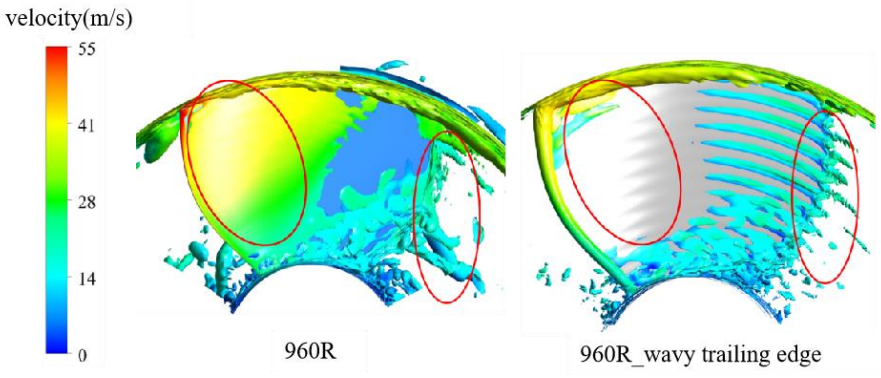

(b)

Fig. 20 Comparison of surface vortex and wake vortex structures of fans: (a) 1100R and 1100R_wavy trailing edge, and (b) 960R and 960R_wavy trailing edge

5. CONCLUSION

This paper introduces an improved method for wavy blade design without altering the blade stagger angle and investigates the impact of wavy configurations with an amplitude of 2% chord length on the aerodynamic noise and performance of two fans with differing chord lengths. The hybrid Computational Aeroacoustics approach was used for the computation of noise and sound propagation, on the basis of transient flow field simulated by using LES. The primary findings can be summarized as follows:

(1) Based on the design conditions, the wavy trailing edge leads to a noise reduction of 2.6 dB for the 1100R fan and 2.1 dB for the 960R fan, while the wavy leading edge results in an overall noise reduction of 1.9 dB for the 1100R fan and 1.5 dB for the 960R fan. The noise reduction effect of the wavy trailing edge is superior.

(2) The characteristics of both fans, whether equipped with wavy leading or trailing edge structures, are slightly changed, marked by increased pressures and reduced efficiencies at medium to low flow rates. Nonetheless, these alterations become negligible as the flow rates increase to medium to high levels.

(3) Both the wavy leading edge and trailing edge structures promote the transition of layered vortices into comb vortices with weak spanwise correlation, which is the primary mechanism behind noise reduction. On the wavy fan blade with a small chord length, the comb structure with low spanwise correlation can still be observed in the wake of the blade. However, on the wavy blade with a large chord length, the comb structure of the shedding vortex rapidly dissipates downstream of the trailing edge.

(4) The wavy configuration noise reduction strategy proposed in this paper holds reference significance for the development of low-noise axial fans.

ACKNOWLEDGEMENTS

This work has been supported by National Science and Technology Major Project (2017-II-0007-0021).

CONFLICT OF INTEREST

The authors declare there are no known conflicts of interest associated with this publication. We confirm that the paper has been read and approved by all named authors and that there are no other persons who satisfied the criteria for authorship but are not listed.

AUTHORS CONTRIBUTION

W. C. Qi: Writing-original draft, Software, Formal analysis; **K. Cheng**: Data Curation, Visualization; **P. C. Li**: Methodology, Visualization; **J. Y. Li**: Methodology, Funding acquisition, Review & Editing.

REFERENCES

Cao, H., Zhang, M., Cai, C., & Zhang, Z. (2020). Flow topology and noise modeling of trailing edge serrations. *Applied Acoustics*, *168*, 107423. https://doi.org/10.1016/j.apacoust.2020.107423

Castegnaro, S. (2018). Aerodynamic design of low-speed axial-flow fans: a historical overview. *Designs*, *2*(3). https://doi.org/10.3390/designs2030020

Cavalieri, A. V. G., Daviller, G., Comte, P., Jordan, P., Tadmor, G. & Gervais, Y. (2011). Using large eddy simulation to explore sound-source mechanisms in jets. *Journal of Sound and Vibration*, *330*(17), 4098-4113. https://doi.org/10.1016/j.jsv.2011.04.018

Valencia, E., Hidalgo, V., Nalianda, D., Laskaridis, P., & Singh, R. (2017). Discretized miller approach to assess effects on boundary layer ingestion induced distortion. *Chinese Journal of Aeronautics*, *30*(1), 235-248. https://doi.org/10.1016/j.cja.2016.12.005

Haeri, S., Kim, J. W., Narayanan, S., & Joseph, P. (2013). *3D calculations of aerofoil-turbulence interaction noise and the effect of wavy leading edges*. AIAA/CEAS Aeroacoustics Conference. https://doi.org/10.2514/6.2014-2325

Hansen, K. L., Kelso, R. M., & Doolan, C. J. (2010). *Reduction of flow induced tonal noise through leading edge tubercle modifications.* AIAA/CEAS Aeroacoustics Conference. https://doi.org/10.2514/6.2010-3700

Hersh, A. S., Soderman, P. T., & Hayden, R. E. (1974). Investigation of acoustic effects of leading-edge serrations on airfoils. *Journal of Aircraft*, *11*, 197-202. https://doi.org/10.2514/3.59219

Howe, M. S. (1991). Aerodynamic noise of a serrated trailing edge. *Journal of Fluids and Structures*, *5*(1), 33-45. https://doi.org/10.1016/0889-9746(91)80010-B

Howe, M. S. (1998). Noise produced by a sawtooth trailing edge. *Acoustical Society of America Journal*, *90*(1), 482-487. https://doi.org/10.1121/1.401273

Koca, K., Genc, M. S., Acikel, H. H., Cagdas, M., & Bodur, T. M. (2018). Identification of flow phenomena over NACA 4412 wind turbine airfoil at low reynolds numbers and role of laminar separation bubble on flow evolution. *Energy*, *144*(FEB.1), 750-764. https://doi.org/10.1016/j.energy.2017.12.045

Krömer, F., Czwielong, F., & Becker, S. (2019). Experimental investigation of the sound emission of skewed axial fans with leading-edge serrations. *AIAA Journal*, *57*(12), 5182-5196. https://doi.org/10.2514/1.J058134

Krömer, F., Renz, A., & Becker, S. (2018). Experimental Investigation of the Sound Reduction by Leading-Edge Serrations in Axial Fans. *AIAA Journal*, *56*, 2086-2090. https://doi.org/10.2514/1.J056355

Lele, S. K., Mendez, S., Ryu, J., Nichols, J., Shoeybi, M.,

& Moin, P. (2010). Sources of high-speed jet noise: Analysis of LES data and modeling. *Procedia Engineering*, *6*, 84-93. https://doi.org/10.1016/j.proeng.2010.09.010

Li, G. P., Ma, Z. L., Chen, C. S., Zhang, Y., Wang, Q., & Chen, E. Y. (2021). *Experimental study on noise reduction characteristics of slanting serrated trailing edge blades.* Journal of Physics: Conference Series, 1885, 042011. https://doi.org/10.1088/1742-6596/1885/4/042011

Lin, J. W., Liu, H. L., Dong, L., Zhou, R. Z., & Hua, R. N. (2022). Analysis of the sound field characteristics of a muffler at different flow conditions. *Journal of Applied Fluid Mechanics*, *16*(1), 147-156. https://doi.org/10.47176/jafm.16.01.1295

Liu, J. M., Zhang, T., & Zhang, Y. O. (2013). Numerical study on flow-induced noise for a steam stop-valve using large eddy simulation. *Journal of Marine Science & Application*, *12*(3), 351-360. https://doi.org/10.1007/s11804-013-1195-9

Nyquist, H. (1928). Certain topics in telegraph transmission theory. *Transactions of the American Institute of Electrical Engineers*, *47*, 617-644. https://doi.org/10.1109/T-AIEE.1928.5055024

Rao, C., Ikeda, T., Nakata, T., & Liu, H. (2017). Owl-inspired leading-edge serrations play a crucial role in aerodynamic force production and sound suppression. *Bioinspiration & Biomimetics*, *12*(4), 046008. https://doi.org/10.1088/1748-3190/aa7013

Sandboge, R., Caro, S., Ploumhans, P., Ambs, R., Schillemeit, B., Washburn, K., & Shakib, F. (2006). *Validation of a CAA formulation based on lighthill's analogy using AcuSolve and ACTRAN/LA on an idealized automotive HVAC blower and on an axial fan*. AIAA/CEAS Aeroacoustics Conference. https://doi.org/10.2514/6.2006-2692

Shur, M. L., Spalart, P. R., & Strelets, M. K. (2011). LES-based evaluation of a microjet noise reduction concept in static and flight conditions. *Journal of Sound & Vibration*, *330*(17), 4083-4097. https://doi.org/10.1016/j.jsv.2011.02.013

Tan, J., Dong, P., Gao, J., Wang, C., & Zhang, L. (2023). Coupling bionic design and numerical simulation of the wavy leading-edge and seagull airfoil of axial flow blade for air-conditioner. *Journal of Applied Fluid Mechanics*, *16*(7), 1316-1330. https://doi.org/10.47176/jafm.16.07.1634

Zhai, C., Tang, Z., Zou, Q., & Qin, L. (2016). Experimental study on the noise characteristics regarding axial auxiliary fans and the noise reduction performance of mufflers. *Arabian Journal for Science & Engineering*, *41*(12), 1-10. https://doi.org/10.1007/s13369-016-2165-8

Zhang, C., Ji, L., Zhou, L., & Sun, S. (2020). Effect of blended blade tip and winglet on aerodynamic and aeroacoustic performances of a diagonal fan. *Aerospace Science and Technology*, *98*, 105688. https://doi.org/10.1016/j.ast.2020.105688

Zhang, Y. O., Zhang, T., & Li, T. Y. (2014). Flow-induced noise simulation based on LES/Lighthill hybrid method. *ICMECS*, 428-431. https://doi.org/10.4028/www.scientific.net/AMM.614.428

Zhou, H., Wang, L., Huang, Z. F., & Ren, J. Z. (2022). Shedding vortex simulation method based on viscous compensation technology research. *Chinese Physics B*, *31*(4). https://doi.org/10.1088/1674-1056/ac29ae

Zhou, S., Li, H., Wang, J., Wang, X., & Ye, J. (2014). Investigation acoustic effect of the convexity-preserving axial flow fan based on bezier function. *Computers & Fluids*, *102*, 85-93. https://doi.org/10.1016/j.compfluid.2014.06.019

Zuo, Z. G., Huang, Q., & Liu, S. (2019). An analysis on the flow field structures and the aerodynamic noise of airfoils with serrated trailing edges based on embedded large eddy flow simulations. *Journal of Applied Fluid Mechanics,* *12*(2), 327-339. https://doi.org/10.29252/jafm.12.02.29142